Applied Catalysis B: Environment and Energy 350 (2024) 123946

Contents lists available at ScienceDirect

Applied Catalysis B: Environment and Energy

journal homepage: www.elsevier.com/locate/apcatb

Converting CO_2 to single-cell protein via an integrated electrocatalytic-biosynthetic system

Huijuan Cui [a,b], Weisong Liu [a,b,c], Chunling Ma [a,b], Pezhman Shiri [a,b], Zhiguang Zhu [a,b,c], Huifeng Jiang [a,c], Demao Li [a,c,*], Lingling Zhang [a,b,c,*]

[a] Key Laboratory of Engineering Biology for Low-carbon Manufacturing, Tianjin Institute of Industrial Biotechnology, Chinese Academy of Sciences, 32 West 7th Avenue, Tianjin Airport Economic Area, Tianjin 300308, China
[b] In Vitro Synthetic Biology Center, Tianjin Institute of Industrial Biotechnology, Chinese Academy of Sciences, Tianjin 300308, China
[c] University of Chinese Academy of Sciences, Beijing 100049, China

ARTICLE INFO

Keywords:
Electrocatalytic CO_2 reduction
Biosynthesis
Cu-based electrocatalyst
Formate
Single cell protein

ABSTRACT

Boosting CO_2 biotransformation by renewable electrical energy provides a prospective avenue to reform the biomanufacturing paradigm and achieve a circular carbon economy. However, mismatches between electrocatalytic and biosynthetic modules lead to poor efficiency. Herein, we design an integrated electro-driven CO_2-single cell protein (SCP) transformation system, via coupling an electrocatalytic CO_2 reduction to formate module with a formate assimilation module. A Cu/Cu_2O electrocatalyst has been rationally designed with excellent duration stability over 100 h under −0.78 V_{RHE}. Strain adaptability investigation and equipment upgrading are carried out to guarantee the effective integration. SCP has been accumulated to a OD_{600} of 4 with an exponential growth rate of 0.114 OD h^{-1} and electrical energy conversion efficiency of 9.2%. No risky hydrogen is needed and the produced formate is ready-to-use for biosynthesis. The elaborate construction bridges non-biological and biological carbon fixation units and offers a promising blueprint for electro-driven CO_2 biotransformation and scalable bio-manufacturing.

1. Introduction

CO_2 transformation is a necessary strategy for simultaneously alleviating the environmental problems and achieving a circular carbon economy [1–4]. Past decades have witnessed remarkable achievements in CO_2 chemical transformation including electrochemical, photochemical, and thermochemical approaches [5–7]. Especially, the hydrogenation of CO_2 to liquid fuels via thermochemical route has realized industrial-class production. The major products of CO_2 chemical transformation are C_1 and C_2 species [8–11]. A long-term goal is direct CO_2 utilization to produce long-chain products, yet challenging due to high C-C coupling energy barrier [12]. Biochemical transformation of CO_2 via biochemical reactions can realize the synthesis of macromolecular products. For instance, Niv Antonovsky et al. synthesized sugars and other major biomass constituents by a fully functional Calvin-Benson-Bassham cycle in *Escherichia coli* [13]. Ni et al. constructed a photoautotrophic platform with the unicellular cyanobacterium *Synechococcus elongatus* PCC7942 to directly convert CO_2 into high-value plant natural products.[14] However, direct CO_2 activation via bio-catalysis is difficult, leading to poor efficiency. Contrarily, utilizing C1/C2 species as substrates in bio-catalytic processes enables efficient and specific production of long-chain products [15]. Integrating chemical transformation and biotransformation provides a feasible way for CO_2 conversion to long-chain products and great achievements have been reported such as synthesis of artificial starch, hexoses and amino acid [16–23]. Compared with thermochemical and photochemical processes, electrochemical route operates under mild conditions and has high efficiency, making it particularly attractive for practical application [16,20,24].

Despite remarkable achievements, hybrid CO_2 biotransformation systems face common challenges of insufficient energy conversion efficiency and sluggish transformation kinetics. In this regards, two main factors should be considered. The first factor is selecting optimal intermediate to bridge electrocatalytic and biosynthetic reactions. C_{2+} products, especially acetate, were chosen as intermediates in previous reports [16,20]. For instance, Zheng et al. selected acetate, via a

* Corresponding authors at: Key Laboratory of Engineering Biology for Low-carbon Manufacturing, Tianjin Institute of Industrial Biotechnology, Chinese Academy of Sciences, 32 West 7th Avenue, Tianjin Airport Economic Area, Tianjin 300308, China.
E-mail addresses: li_dm@tib.cas.cn (D. Li), zhangll@tib.cas.cn (L. Zhang).

https://doi.org/10.1016/j.apcatb.2024.123946
Received 7 December 2023; Received in revised form 4 February 2024; Accepted 9 March 2024
Available online 12 March 2024

CO_2-CO-acetate pathway, as the intermediate to bridge electrocatalytic CO_2RR and biosynthesis of glucose and fatty acid. The final energy efficiency (EE) is 0.65% [20]. Apparently, acetate is not an optimal intermediate from the view of EE, as acetate metabolic pathway in microorganism is an energy-consuming process. The other factor is the compatibility between electrocatalysis and biosynthesis modules. Generally, biosynthetic modules require cations (e.g., Ca^{2+} and Mg^{2+}) to facilitate biochemical reactions, which may deactivate electrocatalysts due to salt deposition. Electrocatalysis prefers electrolyte with higher pH and ionic intensity (e.g., 1 M KOH), while biosynthesis is often implemented in mild buffer like neutral pH and low-salinity. Consequently, two separate units are typically employed. The produced intermediates in the chemical phase necessitate additional separation and purification before entering the biological phase, thereby complicating the entire process and increasing costs [16,20]. Therefore, it is crucial to explore appropriate electrocatalysts to fulfill the requirements of certain intermediate and sufficient biocompatibility.

Recent techno-economic analysis suggests that electrochemical synthesis of CO or formic acid/formate is more feasible than C_{2+} products due to high production rate and superior adaptability for future industrial implementation [25]. In bio-manufacturing, soluble formate is one of the most important one-carbon substrates, metabolized by a broad range of organisms. Bismuth-based materials have been well-known to possess the highest electrocatalytic activity towards formate production with excellent selectivity [25–27]. However, their industrial applications are constrained by their limited long-term stability (typically less than 20 h) and low abundance on Earth ($2*10^{-5}$%) [25,28,29]. Copper is a transition metal element with high earth abundance (10^{-2}%) and copper-based materials have been validated as potential candidates for CO_2 reduction to formate [30,31]. Particularly, both theoretical and experimental studies have shown that formate can be preferably generated over copper(I) oxide Cu_2O(111) due to the low energy barrier for forming critical bidentate HCOO* intermediate [32,33]. Unfortunately, the formate faradic efficiency (FE) over Cu_2O decayed quickly, making it critical yet challenging to rationally design high-stability Cu_2O-based electrocatalysts.

With the increasing global demand for protein, single-cell proteins (SCP), also termed as microbial protein, have attracted intensive attentions due to their high protein contents and complete amino acid ingredients [34,35]. Compared with animal- and plant-derived dietary proteins, SCP processes additional advantages like environmentally benign production and superfast growth rate. Moreover, some protein-abundant microorganisms are even autotrophic, which utilize CO_2 as the feedstock [36,37]. Hydrogen-oxidizing bacteria represent a type of autotrophs with CO_2, O_2, and H_2 as the nutrient/energy supply [35,38]. Obviously, the co-supply of O_2 and H_2 may cause safety concerns, and the low solubility of CO_2 and H_2 increases difficulties in bioreactor design and industrial application. In this circumstance, C_1-assimated SCP-microorgamisms might be optimal alternatives, where C_1 intermediate can be derived from CO_2 electroreduction. *Paracoccus communis* MA5, isolated from soil, demonstrates excellent ability to synthesize SCP from formate [34,39]. The growth rate reaches 0.11 OD_{600} h^{-1} with 5 g L^{-1} formate and 8 g L^{-1} nitrogen source supply [39]. Thus, it holds great promise to couple electrocatalytic CO_2-formate conversion with formate-assimated *Paracoccus communis* MA5 cultivation, which has not been reported yet.

Herein, we describe an electrocatalytic-biosynthetic integrated system (EBIS) for high-rate production of SCP from CO_2 via coupling an electrocatalytic CO_2RR to formate module with a formate-assimilated *Paracoccus communis* MA5 module. A high-stable Cu/Cu_2O electrocatalyst was first designed and prepared for continuous conversion of CO_2 into formate. Then, the compatibility between electrocatalysis and biosynthesis module was studied to ensure effective integration. After optimization, the constructed EBIS realizes seamless and continuous SCP production with CO_2 as the sole carbon source and no H_2 is needed, decreasing security risks and manufacturing costs. This system offers a paradigm for biosynthesis and plentiful products can be synthesized via adjusting the modules, demonstrating its broad prospects in carbon fixation and bio-manufacturing.

2. Experimental

2.1. Material synthesis and electrode preparation

Cu/Cu_2O catalysts were prepared by simple annealing and electrodeposition. In the first step, a mixture of 0.756 g mercaptosuccinic acid, 1.718 g $CuCl_2$·2 H_2O, 1.88 g KCl, and 1.475 g NaCl was loaded into a graphite crucible. The crucible was then placed into a horizontal tube furnace for annealing. The annealing was carried out at 900 °C for 2 h with a rate of 5 °C min^{-1} under Ar atmosphere. After cooling, the collected product was further purified by washing with deionized water to remove soluble salt. The purified product was then dried at 60 °C for 24 h. The final product obtained through this procedure was identified as Cu_2S powder.

In the electrodeposition step, a platinum sheet and a Hg/Hg_2SO_4 electrode were employed as counter and reference electrodes, respectively. The working electrode was carbon paper electrode (1 cm^2) coated with the prepared Cu_2S powder (1 mg cm^{-2}). For the H-cell and flow-cell setups, Toray TGP-H-060 and SGL 22BB carbon papers were utilized, respectively. Typically, a uniform catalyst ink was prepared by mixing 10 mg of active materials, 50 μL of 5 wt% Nafion solution, 200 μL of ethanol, and 250 μL of deionized water. Subsequently, 50 μL of the ink solution was carefully deposited onto the carbon paper and air-dried at room temperature. The electrodeposition process was then conducted at −1.0 V vs. Hg/Hg_2SO_4 for 1000 s in 0.05 M H_2SO_4 containing 5 mM $CuSO_4$ under Ar atmosphere. All reagents were used as received, with analytical grades.

2.2. Material characterization

The structures and morphologies of the synthesized samples were analyzed using field emission scanning electron microscopy (JSM-7800) and high-resolution transmission electron microscopy (JEM-2800). X-ray diffraction test was performed on a Rigaku XtalAB PRO MM007 DW system. The elemental compositions of the samples were characterized via X-ray photoelectron spectroscopy and auger electron spectroscopy (Axis Ultra DLD). A Thermo Nicolet 6700 spectrometer equipped with MCT detector cooled by liquid nitrogen was employed for electrochemical ATR-SEIRAS measurements.

2.3. Electrochemical measurements

All electrochemical measurements were conducted on a CHI 760E electrochemical workstation (CH Instrument, Shanghai, China). Both H-cell and flow-cell systems were used to study the electrochemical performance with Cu-based electrocatalyst coated carbon paper as the working electrode, Ag/AgCl as the reference electrode and Pt sheet as the counter electrode. Anode and cathode chambers were filled with 30 mL 0.5 M $KHCO_3$ electrolytes and separated by Nafion 212 membrane.

In the H-cell system, prior to the tests, the catholyte was saturated by bubbling CO_2 for at least 30 min at a flow rate of 20 mL min^{-1}. Cyclic voltammograms were recorded at a scan rate of 50 mV s^{-1} in CO_2 or Ar atmosphere from 0 to −1.4 V vs. RHE. The equation of E (vs. RHE) = E (vs. Ag/AgCl) + 0.197 V + 0.0591 × pH was used to convert electrode potentials to the reversible hydrogen electrode (RHE) scale. Electrochemical CO_2 reduction reaction (CO_2RR) was evaluated by electrolysis at each given potential for 60 min.

In the flow-cell system, a mass flow meter was used to control CO_2 flow at 40 mL min^{-1}. Electrolyte was circulated through the electrochemical cell by using peristaltic pumps with a silicone tubing, maintaining a flow rate of 5 mL min^{-1}. Electrochemical performance was

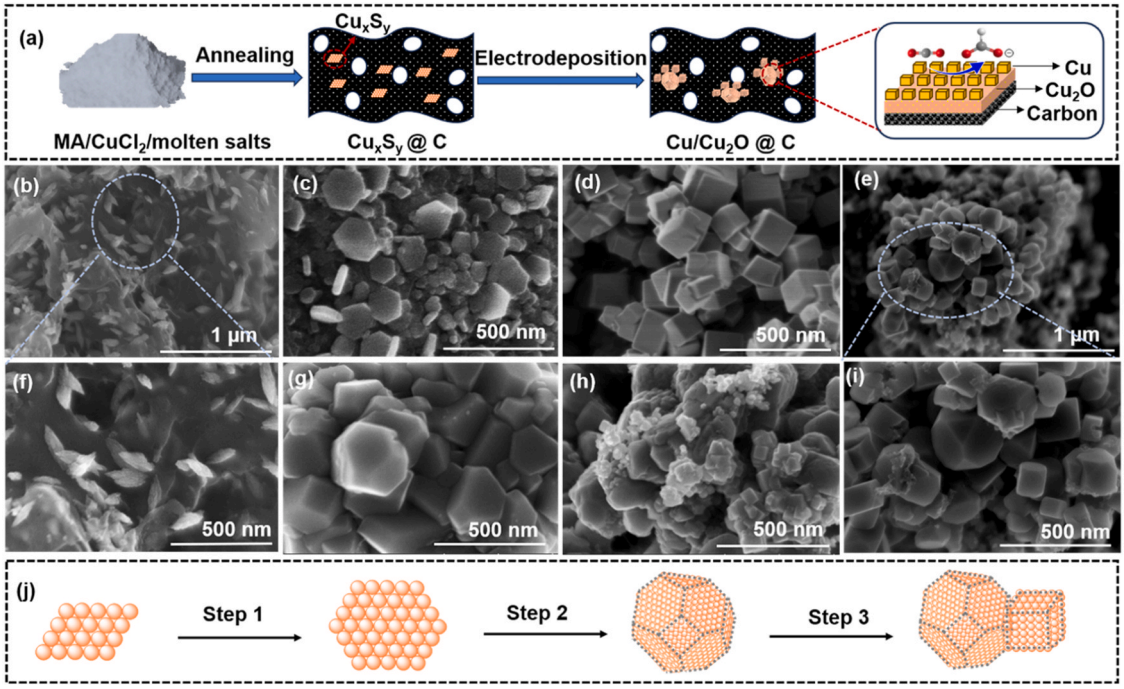

Fig. 1. Design and synthesis of Cu/Cu_2O electrocatalyst. (a) A schematic diagram of design and synthesis of Cu/Cu_2O electrocatalyst. (b-i) SEM images of different Cu-based materials. (b, f) Irregular sheet-like Cu_2S prepared via annealing. (c) Treatment of Cu_2S in 0.05 M H_2SO_4 electrolyte. (d) Direct electrodeposition of $CuSO_4$ on carbon paper. (g) Electrodeposition 200 s, (h) 500 s, and (e, i) 1000 s of $CuSO_4$ on Cu_2S coated carbon paper. (j) A schematic diagram of the possible formation mechanism for Cu/Cu_2O.

assessed through controlled potential electrolysis at each given potential for 30 min. For stability test, the experiment was carried out under −0.78 V_{RHE} for 100 h, with catholyte and anolyte volumes of 100 mL and 400 mL, respectively.

Gas products were analyzed using a gas chromatograph (GC, Shimadzu GC-2014) equipped with a thermal conductivity detector (TCD) and two flame ionization detectors (FID). H_2 was detected using TCD, while carbon monoxide (CO) and methane (CH_4) were analyzed by FID1, and ethylene (C_2H_4) by FID2. Liquid products were analyzed via high-performance liquid chromatography (HPLC, Shimadzu LC-20A) with a differential refractive index detector and 600 MHz nuclear magnetic resonance spectrometer (^{1}H NMR, Bruker AVANCE III 600 MHz). HPLC was used to quantify formate product according to calibration curves with 5 mM H_2SO_4 as mobile phase and BIO-RAD Aminex HPX-87 H as analytical column. The test was carried out at 60 °C with a flow rate of 0.6 mL min^{-1} for 20 min, with a retention time of formate at approximately 14 minutes. ^{1}H NMR was used to qualitatively analyze the liquid product composition. 400 μL of liquid products was mixed with 150 μL of D_2O/tris(trimethylsilyl) phosphate mixtures (TMSP, 0.05%) and 50 μL of 5 mM DMSO to form standard solutions. The peak position of formate is about 8.4 ppm.

2.4. Strain and culture conditions

Paracoccus communis strain MA5 was pre-cultured in LB medium (consisting of 10 g L^{-1} tryptone, 5 g L^{-1} yeast extract and 10 g L^{-1} NaCl) overnight at 37 ℃ and then inoculated into its growth medium. The original growth medium contained 4 g L^{-1} HCOOK, 0.208 g L^{-1} $(NH_4)_2SO_4$, 0.5 g L^{-1} NaCl, 0.5 g L^{-1} KCl, 0.5 g L^{-1} $MgCl_2{\cdot}6\ H_2O$, 0.1 g L^{-1} $CaCl_2{\cdot}2\ H_2O$, and 0.2 g L^{-1} KH_2PO_4.

To investigate the adaptability of *Paracoccus communis* MA5 strain in $KHCO_3$-contained medium, different amounts of $KHCO_3$ were added into the original medium with concentrations of 0.1, 0.25, and 0.5 M. Typically, 10 μL of the pre-cultured strain was inoculated into 500 μL of the $KHCO_3$-contained medium and grown at 37 ℃ for 24 h in 96-well plates. Cell growth was monitored by measuring the OD_{600} using an ultraviolet and visible spectrophotometer (BioSpectrometer basic). Each experiment was conducted in triplicate.

2.5. Construction of electrocatalytic-biosynthetic integrated system

The integrated system contains the electrocatalysis and the biosynthesis modules. 0.1 M $KHCO_3$-contained medium was chosen as the catholyte and culture medium, circulated through both the cathode and biosynthesis chambers. A filter membrane (Whatman grade 1 filter paper) separated the two chambers, preventing microbes from entering the circulation.

In the electrocatalysis unit, a modified conventional flow-cell system was employed for effective integration. A two-electrode flow-cell system with electrode area of 2*2 cm^2 and serpentine channels was utilized to increase formate production. On the cathode side, 60 sccm humidified CO_2 was supplied on the back side of GDE for gas diffusion and an anion-exchange membrane (AEM, Sustainion X37–50 RT, Dioxide Materials) was attached to the catalyst layer to prevent cations deposition on the cathode. 50 mL 0.1 M $KHCO_3$-contained medium was used as catholyte. On the anode side, Ni foam was used for water oxidation and 400 mL 0.5 M $KHCO_3$ was used as electrolyte. A proton exchange membrane (PEM, N212, Dupont) was placed on the top of Ni foam for proton exchange. Between the AEM and the PEM, a middle chamber was placed to allow salt solution flow through the chamber and bring the liquid products to the bioconversion unit. Electrochemical test was conducted on a CHI 760E electrochemical workstation with a constant current of 50 mA. Prior to strains inoculation, the electrolyzer operated for 3 h to accumulate a certain amount of formate (approximately13 mmol L^{-1}).

In the biosynthesis unit, 1 mL of strain was inoculated into 50 mL 0.1 M $KHCO_3$-contained medium after 3 h of CO_2RR and maintained at 37 °C and 800 rpm using a heating magnetic stirrer for growth. Cell growth was monitored by measuring the OD_{600}. The initial OD_{600} was set as 0.2. After growing for 45 h, cells in the biosynthesis unit were collected by centrifuge (8000 rpm, 10 min), washed, and lyophilized to

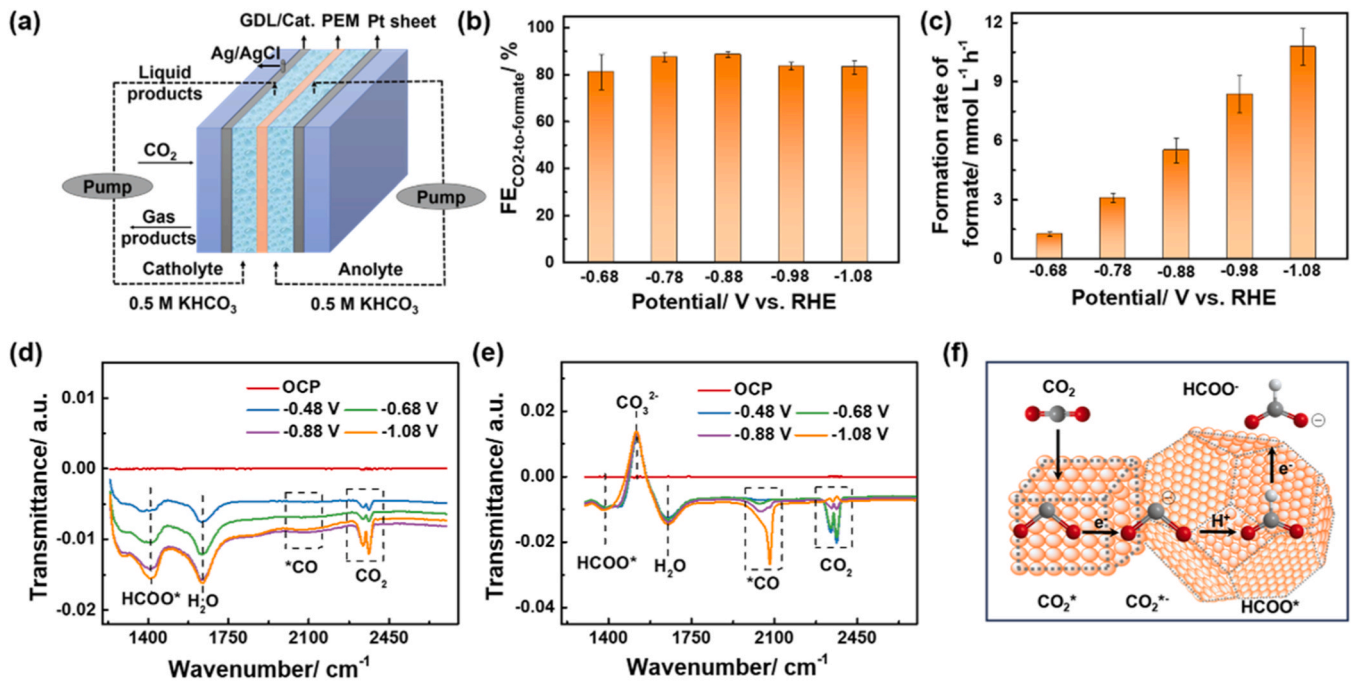

Fig. 2. Electrocatalytic performance and mechanism of Cu/Cu_2O for CO_2RR. (a) Schematic diagram of the three-electrode flow cell. (b) $FE_{CO2\text{-}to\text{-}formate}$ and (c) formation rates of formate in broad potential ranges from −0.78 to −1.08 V_{RHE}. In-situ ATR-SEIRAS of (d) Cu/Cu_2O and (e) Cu electrocatalysts during CO_2RR under different potentials. (f) Schematic diagram of possible CO_2 reduction path for formate formation on Cu/Cu_2O surface.

record the cell dry weight.

3. Results and discussion

3.1. The rationale of Cu/Cu_2O electrocatalyst design and synthesis

3.1.1. Electrocatalyst design

Cu-based material is selected as the aimed electrocatalyst owing to its high abundance and broad application for CO_2RR. Formate selectivity and catalyst stability are two key factors in catalyst design. Previous reports have shown that Cu_xS_y exhibits catalytic activity in converting CO_2 to formate [31,40]. However, S in Cu_xS_y is apt to leach out, resulting in poor stability lasting less than 30 h [33]. Conversely, using Cu_2O derived from Cu_xS_y as the electrocatalyst for CO_2 reduction can improve durability while maintaining formate selectivity. The partial reduction of Cu_2O is one of the major reasons for stability decreasing. Adding a carbon-protected layer can further enhance the stability of Cu-based catalyst [41]. Additionally, growing a layer of Cu on the surface of Cu_2O can prevent it from reduction as well promote CO_2 adsorption [42]. Based on the above analysis, a Cu/Cu_2O nanocomposite supported on porous carbon is designed to maintain formate selectivity and long-term durability for subsequent growth of SCP (Fig. 1a).

3.1.2. Electrocatalyst preparation and characterization

The designed catalyst was synthesized by simple annealing and electrodeposition (Fig. 1a). The morphology and crystal structure were characterized using scanning electron microscopy (SEM) and X-ray diffraction pattern (XRD). Initially, mixtures of mercaptosuccinic acid (MA) and copper chloride were converted into irregular sheet-like Cu_2S (PDF 26–1116) supported on porous carbon after annealing (Figs. 1b and 1f, Fig. S1 and S2). The existence of molten salts can promote the formation of porous carbon supports which is favorable for mass transportation [43]. After electrodeposition of 1000 s, a nanocomposite of Cu/Cu_2O was synthesized with a structure of cubic Cu (PDF 04–0836) capped polyhedral Cu_2O (PDF 05–0667) (Figs. 1e and 1i, Fig. S1 and S3). These structures and compositions are further verified by transmission electron microscopy (TEM), X-ray photoelectron spectroscopy (XPS), and Auger electron spectroscopy (AES) of Cu LMM signal (Fig. S4-6 and Table S1).

To gain deeper insights into the formation mechanism of the prepared Cu/Cu_2O, several control materials were synthesized and analyzed. When the irregular sheet-like Cu_2S undergoes electrochemical treatment at −1.0 V (vs. Hg/Hg_2SO_4) for 1000 s in 0.05 M H_2SO_4 (Cu_2S@CP-1000), its morphology changes into regular hexagons, indicating structure reconstruction (Fig. 1c). XRD result shows that the reconstructed material maintains the composition and crystalline feature of Cu_2S (Fig. S7). The decreased peak intensity at 46 and 49 degree, compared to Fig. S1, may result from S atom leakage [33]. When 0.05 M H_2SO_4 containing 5 mM $CuSO_4$ is used as the electrolyte, a polyhedral morphology appears after 200 s electrodeposition, with the coexistence of Cu, Cu_2O and Cu_2S (Fig. 1g and Fig. S8). Owing to the electrodeposition of Cu, the S leakage rate decreases and the vacant Cu^+ reacts with oxygen atom to form Cu_2O. With a further increase in electrodeposition time to 500 s, small nanocubes form on the surface of the polyhedrons (Fig. 1h). The peaks of Cu_2S disappear, while the peak intensities of Cu and Cu_2O increase remarkably (Fig. S8). Thus, it is deduced that Cu_2S has been completely transformed into Cu_2O. After deposition for 1000 s, it is observed that the underlying Cu_2O polyhedrons have been shielded by the increased Cu nanocubes in size (Figs. 1e and 1i). As a control, when no Cu_2S is used, the electrodeposited Cu nanocubes grow directly on the surface of carbon paper (Fig. 1d and Fig. S1). Based on the above observations, a possible three-step formation mechanism for Cu/Cu_2O has been proposed (Fig. 1j). Initially, the irregular sheet-like Cu_2S is reconstructed into regular hexagon Cu_2S; afterwards, regular hexagon Cu_2S is converted into polyhedral Cu_2O; and finally, cubic Cu is grown on the surface of polyhedral Cu_2O.

3.2. Performance of Cu/Cu_2O electrocatalyst and possible electrocatalytic mechanism

3.2.1. Electrocatalytic performance

The electrocatalytic performance of Cu/Cu_2O nanocomposite

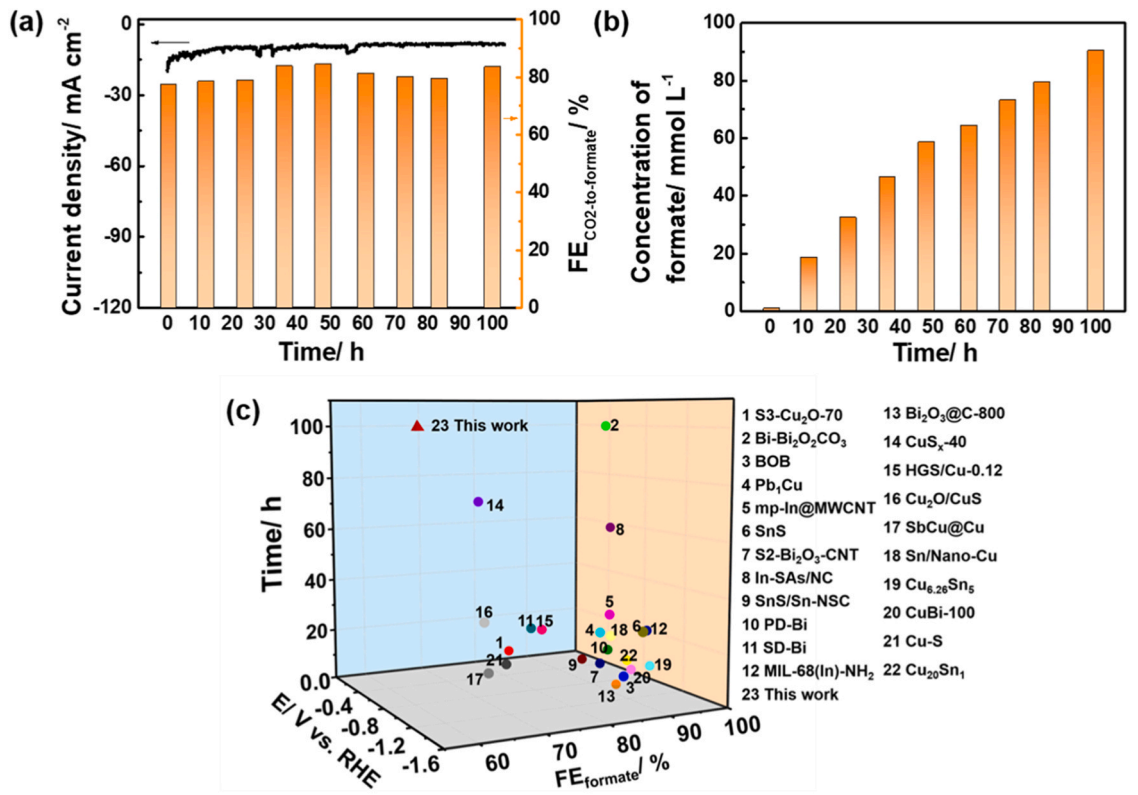

Fig. 3. Stability of Cu/Cu_2O for CO_2RR. (a) $FE_{CO2\text{-}to\text{-}formate}$ and (b) concentrations of formate during 100 h test at −0.78 V_{RHE}. (c) Performance comparison with the reported electrocatalysts.

towards CO_2RR was first investigated using an H-type cell with a typical three-electrode configuration. Considering that most biosynthesis is implemented in mild buffers like neutral pH, 0.5 M $KHCO_3$ was chosen as the electrolyte in the preliminary assay instead of the defined KOH. Cyclic voltammetry was used to estimate the activity of Cu/Cu_2O electrocatalyst. As shown in Fig. S9, the catalytic current at −1.38 V_{RHE} responding to saturated CO_2 is 16 mA cm^{-2}. The electroreduction products were quantified using both gas chromatography (GC) and high-performance liquid chromatograph (HPLC). At the potential of −0.78 V_{RHE}, the $FE_{formate}$ of the optimized Cu/Cu_2O electrocatalyst (Cu_2S-Cu-1000 s) achieves 54%, much higher than that of Cu (7.9%) and Cu_2S (16%) (Fig. S10 and S11). More importantly, formate is the sole liquid product, consistent with the result of nuclear magnetic resonance (NMR) spectroscopy (Fig. S12 and S13). This characteristic would streamline practical applications by eliminating the need for post-separation. Unless stated, the Cu/Cu_2O used later was prepared after electrodeposition of 1000 s.

A gas diffusion electrode (GDE) flow cell was further used to mitigate the side reaction of hydrogen evolution and circumvent the gas solubility limitation of CO_2 in the aqueous electrolyte (Fig. 2a). The Cu/Cu_2O electrocatalyst delivers an enhanced selectivity for formate formation with high $FE_{CO2\text{-}to\text{-}formate}$ of over 80% in broad potential ranges from −0.68 to −1.08 V_{RHE} (Fig. 2b and Fig. S14). The formation rate of formate increases from 1 to 11 mmol L^{-1} h^{-1} (about 0.1–0.9 g L^{-1} h^{-1}) at the potentials of −0.68 to −1.08 V_{RHE} (Fig. 2c), meeting the requirements for *Paracoccus communis* MA5 growth (Fig.S15).

3.2.2. *Electrocatalytic mechanism of CO_2-to-formate*

In-situ ATR-SEIRAS measurements were conducted to explore the CO_2RR pathway on Cu/Cu_2O electrocatalyst (Fig. 2d-e). Spectra were collected from −0.48 to −1.08 V_{RHE} with measurement at open circuit potential (OCP) as the reference. As shown in Fig. 2d, the characteristic peaks at about 2330 cm^{-1} and 1640 cm^{-1} are ascribed to the asymmetric O-C═O vibration of adsorbed CO_2 and the bending of H-O-H in water, respectively.[44,45] The peak near1400 cm^{-1} is assigned to a bidentate HCOO* species with two oxygens coordinated on Cu atoms, crucial intermediates for formate generation.[44,46,47] No obvious peaks at 1900–2100 cm^{-1} for CO* is detected, indicating negligible CO formation on the Cu/Cu_2O electrode.[44] For comparison, the electrocatalyst of directly deposited Cu was also examined (Fig. 2e). Notably, a sharp band at 2070 cm^{-1} with a shoulder at 2040 cm^{-1} appears, interpreted as the low-frequency band and the high-frequency band of atop-bound CO, respectively.[48] Besides, the reversal peak at 1517 cm^{-1} is assigned to the desorption of surface-adsorbed carbonate anions, which can form during CO_2 reduction to CO.[48] Carbonate desorption correlates directly with CO adsorption on the surface of Cu.[49] Its peak strengthens with increased CO adsorption on the surface of Cu-based electrocatalyst. These results indicate that directly deposited Cu follows CO formation pathway. Based on these findings, a possible CO_2 reduction path to formate is speculated in Fig. 2f. Firstly, CO_2 molecule absorbs onto the surface of Cu. Previous report has shown that the Cu(111) facet is favorable for CO_2 adsorption [42]. Secondly, the adsorbed CO_2 molecule is activated into CO_2^{*-} species by accepting one electron, which then capture one proton to produce HCOO* intermediate at the interfaces of Cu and Cu_2O. Finally, HCOO* further reacts with another electron to form $HCOO^-$ and desorbs from the catalyst surface.

3.3. *Studies on the compatibility between electrocatalytic module and biosynthesis module*

3.3.1. *Catalyst stability*

Biomanufacturing usually needs tens to hundreds of hours for single-batch production. Most reported electrocatalysts for CO_2RR to formate fail to meet this requirement, thereby limiting their practical application (Table S2). In the investigation of long-term stability, the synthesized

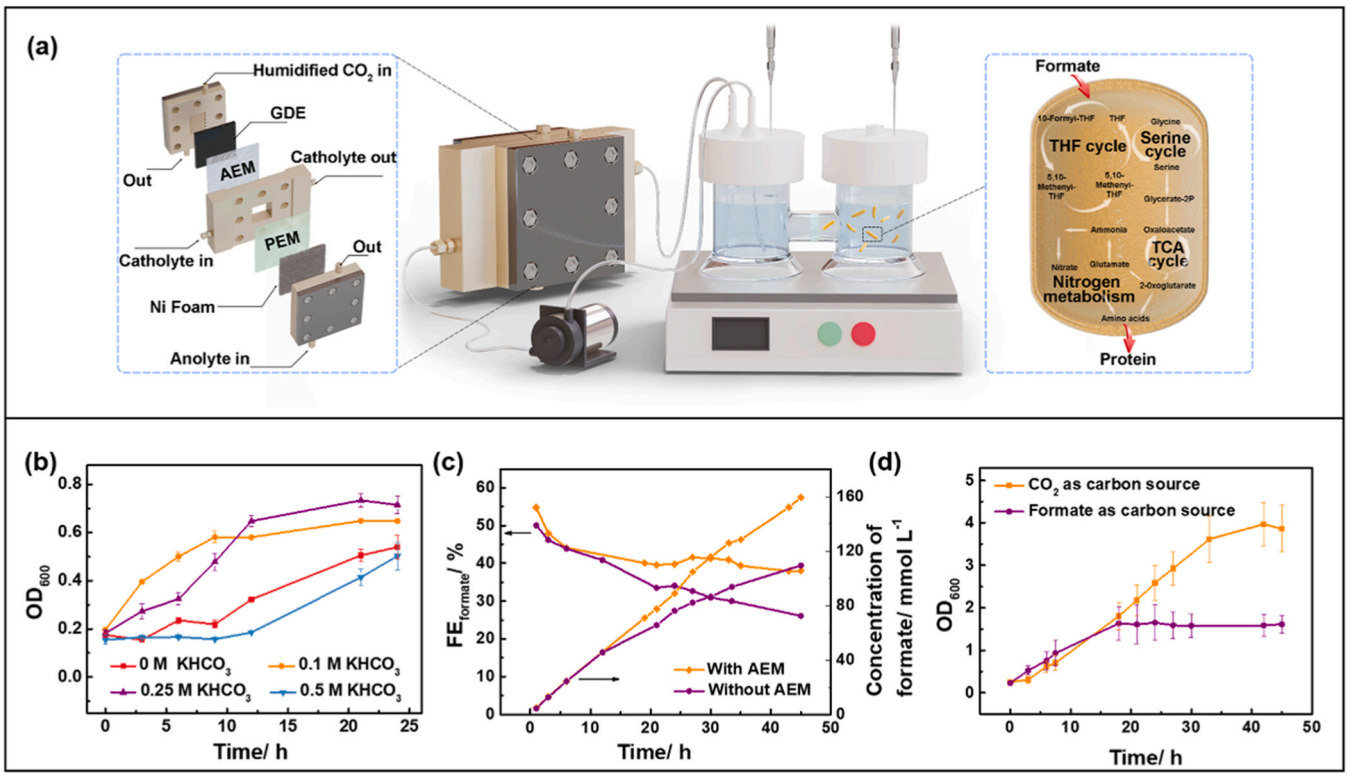

Fig. 4. System integration and application for SCP production. (a) Schematic diagram of the electrocatalytic–biosynthetic integrated system. (b) Adaptability investigation of *Paracoccus communis* MA5 strain in $KHCO_3$-contained medium. (c) FEs and concentrations of formate achieved with and without use of AEM on electrocatalyst surface. (d) Strain growth monitoring with CO_2 or formate as the initial carbon sources.

Cu/Cu_2O electrocatalyst produces up to 90 mmol L^{-1} (~4.7 mol g_{cat}^{-1}) formate at −0.78 V_{RHE} over 100 h, with a stable $FE_{CO2\text{-}to\text{-}formate}$ of approximately 80% (Figs. 3a, 3b, and Fig. S16), exceeding most of the reported electrocatalysts towards CO_2RR to formate (Fig. 3c and Table S2). Further characterization reveals that the crystalline phase of Cu_2O does not change significantly even after 100 h (Fig. S17). It is speculated that the excellent stability of Cu_2O under CO_2RR is attributed to the special preparation processes. Both the Cu_2S-derived Cu_2O process in the porous carbon and the electrodeposition of Cu on the surface of Cu_2O prevent its reduction and enhance stability, indicating the rationality of the catalyst design.

3.3.2. *Adaptability investigation of Paracoccus communis MA5 in $KHCO_3$-contained medium*

The influence of $KHCO_3$ concentration on strain growth is studied via supplementing the defined cultivation medium with different amounts of $KHCO_3$ (Fig. 4b). Fortunately, $KHCO_3$ concentrations of 0.1 M and 0.25 M accelerated the initial growth of *Paracoccus communis* MA5 strain and increased the final quantity of stain accumulation. When the concentration increased to 0.5 M, the initial growth rate was suppressed, despite no influence on the OD value after cultivation for 25 h. It is assumed that the initial inhibition resulted from excessive pH or salinity. Eventually, 0.1 M $KHCO_3$ was chosen to add into the culture medium.

3.3.3. *Equipment upgrading to solve the interferences between electrocatalytic module and biosynthesis module*

Biosynthetic processes require cations to facilitate biochemical reactions, potentially leading to electrocatalysts deactivation due to salt deposition during the electroreduction process. In this study, Ca^{2+} and Mg^{2+} are contained in the culture medium. As shown in Fig. S18, when the 0.1 M $KHCO_3$-contained medium is used as electrolyte for CO_2RR, $CaCO_3$ forms on the surface of cathode. To decrease the impact of bioconversion media on electrocatalysis, a membrane-integrated cathode was designed by installing an anion exchange membrane (AEM) onto Cu/Cu_2O electrocatalyst surface [17]. When AEM is used, humidified CO_2 is needed to generate current. However, the current is lower than 10 mA cm^{-2} even at −1.38 V_{RHE} in the flow-cell system used above (Fig. S19). To increase the current, we upgrade the flow cell to a two-electrode flow-cell system with an increased electrode area of 2*2 cm^2 and serpentine channels (Fig. 4a). Fig. 4c shows the comparison before and after equipment upgrading, and the higher FE value and formate yield after 45 h suggests the robustness of the setup as well as the protective effect of AEM against mineral ion deposition. It is concerned that the electrocatalytic factors such as applied voltage, increased local pH around electrodes and shear force during buffer stirring may be incompatible with the biosynthesis module. A two-chamber cell with a filter membrane has been employed to segregate microbes into a separate chamber.

3.4. *Integration of electrocatalytic module and biosynthesis module*

The EBIS system, consisting of the CO_2 electroreduction unit and the biosynthesis unit, was constructed to produce SCP from CO_2 after overcoming the above difficulties (Fig. 4a). As CO_2 is the sole carbon source, the electrocatalytic unit needs to run for 3 h under a constant current of 50 mA to accumulate sufficient formate (13 mmol L^{-1}) to initiate SCP production in the biosynthesis unit (Fig. S20). Three photographs of the EBIS are given in Fig. S21, clearly displaying the growth of *Paracoccus communis* MA5 strain. The OD_{600} value reaches up to 4 after 42 h, which is even two-times higher than that of direct growth with formate as the sole carbon source (Fig. 4d). The possible reason is deduced as that continuous formate production from CO_2 works like fed-batch cultivation, guaranteeing slow changes in pH or salt concentration and promoting rapid microorganism growth. The collected cell dry weight is determined as 2.6 g L^{-1} with a protein content of 45%, comparable to soybean protein content. It is predicted that protein content

Table 1
Comparison of cell growth rate in the EBIS with other electro-microbial systems.

Number	General CO_2 conversion route	Microorganism	Electro-bio integration	Continuous production	CO_2 as sole carbon source	No H_2	Cell growth rate (OD h^{-1})[a]	Reference
1	CO_2-to-acetate-to-glucose	*Saccharomyces cerevisiae*	√	×	×	√	0.031	Ref. [20]
2	CO_2-to-acetate-to- food	*Saccharomyces cerevisiae*	√	×	×	√	0.108	Ref. [16]
3	CO_2-to-C_{2+}-to-PHA	*Pseudomonas putida*	√	√	×	√	0.105	Ref. [17]
4	CO_2 to acetate	*Sporomusa ovata*	√	√	√	×	0.002	Ref. [36]
5	CO_2-to-PHB	*Ralstonia eutropha*	√	√	×	×	0.012	Ref. [50]
6	CO_2-to-syngas (CO)-to-butanol /hexanol	*Clostridium autoethanogenum & Clostridium kluyveri*	√	×	×	×	0.025	Ref. [51]
7	CO_2-to-formate-to-SCP	*Paracoccus communis* MA5	√	√	√	√	0.114	This work

Note a: the rate indicates the exponential growth rate.

can be further improved through replenishing nitrogen source and manipulating the intracellular nitrogen metabolism via metabolic engineering approach. The exponential cell growth rate reached up to 0.114 OD h^{-1}, exceeding most of the electro-bio integrated system (Table 1). As a comparison, an experiment was also carried out without electricity input. The MA5 strain failed to grow with CO_2 as the sole carbon source due to a lack of reducing power.

The EE of electricity to SCP is calculated based on the ratio of the heat contained in SCP (biomass) and the consumed electrical energy (see Supporting information). An $EE_{electricity\text{-}to\text{-}biomass}$ of 9.2% is achieved, surpassing previous results [17,20]. When calculated based on the protein content (45%), the EE value from electricity to protein is 3.4%. This EE can be further enhanced via system optimization. Adding AEM on the surface of electrocatalyst can increase the energy consumption of the entire system. Based on our result, $CaCO_3$ is the sole deposited species that can block the active sites on electrocatalyst (Fig. S18). When no Ca^{2+} is used in the growth medium, AEM is unnecessary in the integrated system. Adjusting the medium composition and selecting optimized strains via adaptive laboratory evolution can realize strain growth without Ca^{2+}. This strategy can be tried to avoid AEM utilization and increase total EE in the future. Together with the advantages in continuous production, sole carbon source, and unnecessity of H_2, the established EBIS is thoroughly superior to other reported systems and holds great promise for scaling up in industrial biomanufacturing.

4. Conclusions

We have demonstrated an EBIS for continuous production of SCP with CO_2 as the sole carbon source via coupling CO_2RR with microbial synthesis. Formate is selected as the intermediate to bridge these two modules due to its proper production rate and superior adaptability for biosynthesis. To meet with continuous formate production for strain growth, a highly stable Cu/Cu_2O electrocatalyst is rationally designed and prepared, which displays a long-term durability over 100 h at −0.78 V_{RHE}, exceeding most reported electrocatalysts. Then, key compatibility issues between electrocatalysis and biosynthesis modules are analyzed and solved to ensure an effective integration, including choosing 0.1 M $KHCO_3$-contained medium as catholyte, installing an AEM on catalyst surface to decrease mineral ions interference and using a two-chamber design with a filter membrane to avoid electrocatalysis interference on microbe growth. With this integrated system, an exponential cell growth rate of 0.114 OD h^{-1} and a cell dry weight accumulation of 2.6 g L^{-1} have been achieved, faster than most reported electro-bio integrated system. The protein content is measured as 45%, which can be further improved via replenishing nitrogen source and manipulating the intracellular nitrogen metabolism pathways. An $EE_{electricity\text{-}to\text{-}biomass}$ of 9.2% has been achieved which can be further enhanced via system optimization. In summary, the established EBIS shows significant advantages over previously reported hybrid system and demonstrates notable technical feasibility for converting CO_2 into SCP. In a broader context, all components of this system can be adjusted and optimized such as electrocatalyst, bridged intermediates, strain, and the related metabolic pathways. This model provides a paradigm to produce value-added macromolecular products from CO_2, thus bringing opportunities in the electricity-driven bio-manufacturing industry.

CRediT authorship contribution statement

Lingling Zhang: Writing – review & editing, Supervision, Funding acquisition, Conceptualization. **Huijuan Cui:** Writing – original draft, Validation, Methodology, Data curation, Conceptualization. **Weisong Liu:** Methodology, Data curation. **Chunling Ma:** Methodology, Data curation. **Pezhman Shiri:** Methodology, Investigation. **Zhiguang Zhu:** Supervision, Conceptualization. **Huifeng Jiang:** Funding acquisition. **Demao Li:** Supervision, Conceptualization.

Declaration of Competing Interest

The authors declare that they have no known competing financial interests or personal relationships that could have appeared to influence the work reported in this paper.

Data availability

Data will be made available on request.

Acknowledgements

This work was supported by Tianjin Synthetic Biotechnology Innovation Capacity Improvement Projects TSBICIP-KJGG-007 and TSBICIP-CXRC-024, and the Strategic Priority Research Program of the Chinese Academy of Sciences XDC0120103 and XDC0110300.

Appendix A. Supporting information

Supplementary data associated with this article can be found in the online version at doi:10.1016/j.apcatb.2024.123946.

References

[1] G. Wang, J. Chen, Y. Ding, P. Cai, L. Yi, Y. Li, C. Tu, Y. Hou, Z. Wen, L. Dai, Electrocatalysis for CO_2 conversion: from fundamentals to value-added products, Chem. Soc. Rev. 50 (2021) 4993–5061.
[2] S. Navarro-Jaen, M. Virginie, J. Bonin, M. Robert, R. Wojcieszak, A.Y. Khodakov, Highlights and challenges in the selective reduction of carbon dioxide to methanol, Nat. Rev. Chem. 5 (2021) 564–579.
[3] E. Gong, S. Ali, C.B. Hiragond, H.S. Kim, N.S. Powar, D. Kim, H. Kim, S.-I. In, Solar fuels: research and development strategies to accelerate photocatalytic CO_2 conversion into hydrocarbon fuels, Energy Environ. Sci. 15 (2022) 880–937.
[4] G. Shang, J. Yu, W. Cai, K. Cui, X. Shen, P. Jin, K. Guo, Comparison of in-situ and ex-situ electrolytic H_2 supply for microbial methane production from CO_2, Bioresour. Technol. 388 (2023) 129728.
[5] B. Seger, M. Robert, F. Jiao, Best practices for electrochemical reduction of carbon dioxide, Nat. Sustain. 6 (2023) 236–238.

[6] Y. Shen, C. Ren, L. Zheng, X. Xu, R. Long, W. Zhang, Y. Yang, Y. Zhang, Y. Yao, H. Chi, J. Wang, Q. Shen, Y. Xiong, Z. Zou, Y. Zhou, Room-temperature photosynthesis of propane from CO_2 with Cu single atoms on vacancy-rich TiO_2, Nat. Commun. 14 (2023) 1117.

[7] H. Xin, L. Lin, R. Li, D. Li, T. Song, R. Mu, Q. Fu, X. Bao, Overturning CO_2 hydrogenation selectivity with high activity via reaction-induced strong metal-support interactions, J. Am. Chem. Soc. 144 (2022) 4874–4882.

[8] B. Sun, M. Dai, S. Cai, H. Cheng, K. Song, Y. Yu, H. Hu, Challenges and strategies towards copper-based catalysts for enhanced electrochemical CO_2 reduction to multi-carbon products, Fuel 332 (2023) 126114.

[9] S. Jin, Z. Hao, K. Zhang, Z. Yan, J. Chen, Advances and Challenges for the electrochemical reduction of CO_2 to CO: from fundamentals to industrialization, Angew. Chem. Int. Ed. 60 (2021) 20627–20648.

[10] J. Wang, G. Li, Z. Li, C. Tang, Z. Feng, H. An, H. Liu, T. Liu, C. Li, A highly selective and stable ZnO-ZrO_2 solid solution catalyst for CO_2 hydrogenation to methanol, Sci. Adv. 3 (2017) e1701290.

[11] Y. Guo, S. Yao, Y. Xue, X. Hu, H. Cui, Z. Zhou, Nickel single-atom catalysts intrinsically promoted by fast pyrolysis for selective electroreduction of CO_2 into CO, Appl. Catal. B-Environ. 304 (2022) 120997.

[12] X. Tan, J. Nielsen, The integration of bio-catalysis and electrocatalysis to produce fuels and chemicals from carbon dioxide, Chem. Soc. Rev. 51 (2022) 4763–4785.

[13] N. Antonovsky, S. Gleizer, E. Noor, Y. Zohar, E. Herz, U. Barenholz, L. Zelcbuch, S. Amram, A. Wides, N. Tepper, D. Davidi, Y. Bar-On, T. Bareia, D.G. Wernick, I. Shani, S. Malitsky, G. Jona, A. Bar-Even, R. Milo, Sugar synthesis from CO_2 in *Escherichia coli*, Cell 166 (2016) 115–125.

[14] J. Ni, F. Tao, Y. Wang, F. Yao, P. Xu, A photoautotrophic platform for the sustainable production of valuable plant natural products from CO_2, Green. Chem. 18 (2016) 3537–3548.

[15] Q. Yang, X. Guo, Y. Liu, H. Jiang, Biocatalytic C-C bond formation for one carbon resource utilization, Int. J. Mol. Sci. 22 (2021) 1890.

[16] E.C. Hann, S. Overa, M. Harland-Dunaway, A.F. Narvaez, D.N. Le, M.L. Orozco-Cárdenas, F. Jiao, R.E. Jinkerson, A hybrid inorganic–biological artificial photosynthesis system for energy-efficient food production, Nat. Food 3 (2022) 461–471.

[17] P. Zhang, K. Chen, B. Xu, J. Li, C. Hu, J.S. Yuan, S.Y. Dai, Chem-bio interface design for rapid conversion of CO_2 to bioplastics in an integrated system, Chem 8 (2022) 3363–3381.

[18] J. Lim, S.Y. Choi, J.W. Lee, S.Y. Lee, H. Lee, Biohybrid CO_2 electrolysis for the direct synthesis of polyesters from CO_2, Proc. Natl. Acad. Sci. U. S. A. 120 (2023) e2221438120.

[19] T. Cai, H. Sun, J. Qiao, L. Zhu, F. Zhang, J. Zhang, Z. Tang, X. Wei, J. Yang, Q. Yuan, W. Wang, X. Yang, H. Chu, Q. Wang, C. You, H. Ma, Y. Sun, Y. Li, C. Li, H. Jiang, Q. Wang, Y. Ma, Cell-free chemoenzymatic starch synthesis from carbon dioxide, Science 373 (2021) 1523–1527.

[20] T. Zheng, M. Zhang, L. Wu, S. Guo, X. Liu, J. Zhao, W. Xue, J. Li, C. Liu, X. Li, Q. Jiang, J. Bao, J. Zeng, T. Yu, C. Xia, Upcycling CO_2 into energy-rich long-chain compounds via electrochemical and metabolic engineering, Nat. Catal. 5 (2022) 388–396.

[21] J. Yang, W. Song, T. Cai, Y. Wang, X. Zhang, W. Wang, P. Chen, Y. Zeng, C. Li, Y. Sun, Y. Ma, De novo artificial synthesis of hexoses from carbon dioxide, Sci. Bull. (2023) 2370–2381.

[22] J. Liu, H. Zhang, Y. Xu, H. Meng, A.P. Zeng, Turn air-captured CO_2 with methanol into amino acid and pyruvate in an ATP/NAD(P)H-free chemoenzymatic system, Nat. Commun. 14 (2023) 2772.

[23] Y.-H.P. Job Zhang, Z. Zhu, C. You, L. Zhang, K. Liu, *In vitro* biotransformation (ivBT): definitions, opportunities, and challenges, Syn, Biol. Eng. 1 (2023) 10013.

[24] H. Wang, J. Xue, C. Liu, Z. Chen, C. Li, X. Li, T. Zheng, Q. Jiang, C. Xia, CO_2 electrolysis toward acetate: a review, Curr. Opin. Electrochem. 39 (2023) 101253.

[25] S. Yang, H. An, S. Arnouts, H. Wang, X. Yu, J. de Ruiter, S. Bals, T. Altantzis, B. M. Weckhuysen, W. van der Stam, Halide-guided active site exposure in bismuth electrocatalysts for selective CO_2 conversion into formic acid, Nat. Catal. 6 (2023) 796–806.

[26] X. Feng, H. Zou, R. Zheng, W. Wei, R. Wang, W. Zou, G. Lim, J. Hong, L. Duan, H. Chen, Bi_2O_3/BiO_2 Nanoheterojunction for highly efficient electrocatalytic CO_2 reduction to formate, Nano Lett. 22 (2022) 1656–1664.

[27] A. Chen, X. Dong, J. Mao, W. Chen, C. Zhu, S. Li, G. Wu, Y. Wei, X. Liu, G. Li, Y. Song, Z. Jiang, W. Wei, Y. Sun, Gas penetrating hollow fiber Bi with contractive bond enables industry-level CO_2 electroreduction, Appl. Catal. B-Environ. 333 (2023) 122768.

[28] S.-Q. Liu, M.-R. Gao, R.-F. Feng, L. Gong, H. Zeng, J.-L. Luo, Electronic delocalization of bismuth oxide induced by sulfur doping for efficient CO_2 electroreduction to formate, ACS Catal. 11 (2021) 7604–7612.

[29] Y. Wang, Y. Li, J. Liu, C. Dong, C. Xiao, L. Cheng, H. Jiang, H. Jiang, C. Li, $BiPO_4$-derived 2D nanosheets for efficient electrocatalytic reduction of CO_2 to liquid fuel, Angew. Chem. Int. Ed. 60 (2021) 7681–7685.

[30] J. Du, Y. Xin, M. Dong, J. Yang, Q. Xu, H. Liu, B. Han, Copper/carbon heterogenous interfaces for enhanced selective electrocatalytic reduction of CO_2 to formate, Small 17 (2021) e2102629.

[31] T. Dou, Y. Qin, F. Zhang, X. Lei, CuS Nanosheet arrays for electrochemical CO_2 reduction with surface reconstruction and the effect on selective formation of formate, ACS Appl. Energ. Mater. 4 (2021) 4376–4384.

[32] S. Wang, T. Kou, J.B. Varley, S.A. Akhade, S.E. Weitzner, S.E. Baker, E.B. Duoss, Y. Li, Cu_2O/CuS nanocomposites show excellent selectivity and stability for formate generation via electrochemical reduction of carbon dioxide, ACS Mater. Lett. 3 (2021) 100–109.

[33] S. Liang, J. Xiao, T. Zhang, Y. Zheng, Q. Wang, B. Liu, Sulfur changes the electrochemical CO_2 reduction pathway over Cu electrocatalysts, Angew. Chem. Int. Ed. (2023) e202310740.

[34] S. Tong, L. Zhao, D. Zhu, W. Chen, L. Chen, D. Li, From formic acid to single-cell protein: genome-scale revealing the metabolic network of *Paracoccus communis* MA5, Bioresour, Bioprocess 9 (2022) 55.

[35] J. Xu, J. Wang, C. Ma, Z. Wei, Y. Zhai, N. Tian, Z. Zhu, M. Xue, D. Li, Embracing a low-carbon future by the production and marketing of C1 gas protein, Biotechnol. Adv. 63 (2023) 108096.

[36] Y. Su, S. Cestellos-Blanco, J.M. Kim, Y.-x Shen, Q. Kong, D. Lu, C. Liu, H. Zhang, Y. Cao, P. Yang, Close-packed nanowire-bacteria hybrids for efficient solar-driven CO_2 fixation, Joule 4 (2020) 800–811.

[37] A. Mishra, J.N. Ntihuga, B. Molitor, L.T. Angenent, Power-to-protein: carbon fixation with renewable electric power to feed the world, Joule 4 (2020) 1142–1147.

[38] B. Pander, Z. Mortimer, C. Woods, C. McGregor, A. Dempster, L. Thomas, J. Maliepaard, R. Mansfield, P. Rowe, P. Krabben, Hydrogen oxidising bacteria for production of single-cell protein and other food and feed ingredients, Eng. Biol. 4 (2020) 21–24.

[39] L. Zhao, D. Zhu, D. Li, Screening and fermentation process of single cell protein-producing strains by formic acid, Feed Res 44 (2021) 88–93.

[40] Y. Deng, Y. Huang, D. Ren, A.D. Handoko, Z.W. Seh, P. Hirunsit, B.S. Yeo, On the role of sulfur for the selective electrochemical reduction of CO_2 to formate on CuS_x catalysts, ACS Appl. Mater. Interfaces 10 (2018) 28572–28581.

[41] M. Fan, J.E. Huang, R.K. Miao, Y. Mao, P. Ou, F. Li, X.-Y. Li, Y. Cao, Z. Zhang, J. Zhang, Y. Yan, A. Ozden, W. Ni, Y. Wang, Y. Zhao, Z. Chen, B. Khatir, C. P. O'Brien, Y. Xu, Y.C. Xiao, G.I.N. Waterhouse, K. Golovin, Z. Wang, E.H. Sargent, D. Sinton, Cationic-group-functionalized electrocatalysts enable stable acidic CO_2 electrolysis, Nat. Catal. 6 (2023) 763–772.

[42] W. Gao, Y. Xu, L. Fu, X. Chang, B. Xu, Experimental evidence of distinct sites for CO_2-to-CO and CO conversion on Cu in the electrochemical CO_2 reduction reaction, Nat. Catal. (2023) 885–894.

[43] H.J. Cui, H.M. Yu, J.F. Zheng, Z.J. Wang, Y.Y. Zhu, S.P. Jia, J. Jia, Z.P. Zhu, N-doped graphene frameworks with superhigh surface area: excellent electrocatalytic performance for oxygen reduction, Nanoscale 8 (2016) 2795–2803.

[44] J. Xue, X. Fu, S. Geng, K. Wang, Z. Li, M. Li, Boosting electrochemical CO_2 reduction via valence state and oxygen vacancy controllable Bi-Sn/CeO_2 nanorod, J. Environ. Manag. 342 (2023) 118354.

[45] M. Wang, S. Liu, B. Chen, M. Huang, C. Peng, Co-regulation of intermediate binding and water activation in sulfur-doped bismuth nanosheets for electrocatalytic CO_2 reduction to formate, Chem. Eng. J. 451 (2023) 139056.

[46] C. Cao, D.D. Ma, J.F. Gu, X. Xie, G. Zeng, X. Li, S.G. Han, Q.L. Zhu, X.T. Wu, Q. Xu, Metal-organic layers leading to atomically thin bismuthene for efficient carbon dioxide electroreduction to liquid fuel, Angew. Chem. Int. Ed. 59 (2020) 15014–15020.

[47] S. Zhu, B. Jiang, W.B. Cai, M. Shao, Direct observation on reaction intermediates and the role of bicarbonate anions in CO_2 electrochemical reduction reaction on Cu surfaces, J. Am. Chem. Soc. 139 (2017) 15664–15667.

[48] M. Moradzaman, G. Mul, Infrared analysis of interfacial phenomena during electrochemical reduction of CO_2 over polycrystalline copper electrodes, ACS Catal. 10 (2020) 8049–8057.

[49] A. Wuttig, J. Ryu, Y. Surendranath, Electrolyte competition controls surface binding of CO intermediates to CO_2 reduction catalysts, J. Phys. Chem. C. 125 (2021) 17042–17050.

[50] C. Liu, B.C. Colon, M. Ziesack, P.A. Silver, D.G. Nocera, Water splitting-biosynthetic system with CO_2 reduction efficiencies exceeding photosynthesis, Science 352 (2016) 1210–1213.

[51] T. Haas, R. Krause, R. Weber, M. Demler, G. Schmid, Technical photosynthesis involving CO_2 electrolysis and fermentation, Nat. Catal. 1 (2018) 32–39.